Eur. J. Biochem. **270**, 3205–3213 (2003) © FEBS 2003 doi:10.1046/j.1432-1033.2003.03692.x

Kinetic characterization, structure modelling studies and crystallization of *Trypanosoma brucei* enolase

Véronique Hannaert[1], Marie-Astrid Albert[1], Daniel J. Rigden[2], M. Theresa da Silva Giotto[3], Otavio Thiemann[3], Richard C. Garratt[3], Joris Van Roy[1], Fred R. Opperdoes[1] and Paul A. M. Michels[1]

[1]*Research Unit for Tropical Diseases, Christian de Duve Institute of Cellular Pathology and Laboratory of Biochemistry, Université Catholique de Louvain, Brussels, Belgium;* [2]*CENARGEN/EMBRAPA, Brasília-D.F., Brazil;* [3]*Instituto de Física de São Carlos, Universidade de São Paulo, São Carlos – SP, Brazil*

In this article, we report the results of an analysis of the glycolytic enzyme enolase (2-phospho-D-glycerate hydrolase) of *Trypanosoma brucei*. Enolase activity was detected in both bloodstream-form and procyclic insect-stage trypanosomes, although a 4.5-fold lower specific activity was found in the cultured procyclic homogenate. Subcellular localization analysis showed that the enzyme is only present in the cytosol. The *T. brucei* enolase was expressed in *Escherichia coli* and purified to homogeneity. The kinetic properties of the bacterially expressed enzyme showed strong similarity to those values found for the natural *T. brucei* enolase present in a cytosolic cell fraction, indicating a proper folding of the enzyme in *E. coli*. The kinetic properties of *T. brucei* enolase were also studied in comparison with enolase from rabbit muscle and *Saccharomyces cerevisiae*. Functionally, similarities were found to exist between the three enzymes: the Michaelis constant (K_m) and K_A values for the substrates and Mg^{2+} are very similar. Differences in pH optima for activity, inhibition by excess Mg^{2+} and susceptibilities to monovalent ions showed that the *T. brucei* enolase behaves more like the yeast enzyme. Alignment of the amino acid sequences of *T. brucei* enolase and other eukaryotic and prokaryotic enolases showed that most residues involved in the binding of its ligands are well conserved. Structure modelling of the *T. brucei* enzyme using the available *S. cerevisiae* structures as templates indicated that there are some atypical residues (one Lys and two Cys) close to the *T. brucei* active site. As these residues are absent from the human host enolase and are therefore potentially interesting for drug design, we initiated attempts to determine the three-dimensional structure. *T. brucei* enolase crystals diffracting at 2.3 Å resolution were obtained and will permit us to pursue the determination of structure.

Keywords: enolase; *Trypanosoma brucei*; kinetics; structure modelling; crystallization.

Enolase (2-phospho-D-glycerate hydrolase, EC 4.2.1.11) catalyses the reversible dehydration of D-2-phosphoglycerate (PGA) to phospho*enol*pyruvate (PEP) in both glycolysis and gluconeogenesis. The enzyme has been studied from a large variety of sources (including Archaebacteria, Eubacteria and Eukaryota) and found to be highly conserved. This conservation is particularly apparent at the catalytic site and has led to enzymes from diverse species sharing many similar kinetic properties. Enolase from all eukaryotes analysed, and from many prokaryotic species, is a dimer, with identical subunits having a molecular mass of 40 000–50 000 [1]; however, octameric enolases have been reported in a variety of bacteria [2,3].

High-resolution crystal structures are known for the enolases from lobster and *Saccharomyces cerevisiae*, both as apoenzyme structures and complexes with substrates and inhibitors [4–7]. These two enolases have very similar amino-acid sequences and three-dimensional structures. Each monomer of enolase contains two domains. The large C-terminal domain is an eightfold α/β barrel of somewhat unusual type, with a topology which differs from that commonly observed in triosephosphate isomerase and many other proteins. The active site of enolase is present at the C terminus of this barrel. The small or N-terminal domain wraps around the outside of the main domain [8]. Most of the intersubunit contacts are between the small domain of one monomer and the large domain of the other. Kinetic experiments have demonstrated that binding of two metal ions to each monomer is required for activity [9–11]. They further suggested the presence of a third, inhibitory,

Correspondence to V. Hannaert, ICP-TROP 74–39, Avenue Hippocrate 74, B-1200 Brussels, Belgium.
Fax: 32 2762 68 53, Tel.: 32 2764 74 72,
E-mail: hannaert@trop.ucl.ac.be

Abbreviations: E-64, 4-[(2*S*,3*S*)-3-carboxyoxiran-2-ylcarbonyl-L-leucylamido]butylguanidine; GAPDH, glyceraldehyde-3-phosphate dehydrogenase; LDH, lactate dehydrogenase; PEP, phospho*enol*pyruvate; PGA, D-2-phosphoglycerate; PGAM, phosphoglycerate mutase; PGK, phosphoglycerate kinase; PYK, pyruvate kinase.

Enzymes: enolase/2-phospho-D-glycerate hydrolase (EC 4.2.1.11); glyceraldehyde-3-phosphate dehydrogenase (EC 1.2.1.12); lactate dehydrogenase (EC 1.1.1.27); phosphoglycerate kinase (EC 2.7.2.3); phosphoglycerate mutase (EC 5.4.2.1); pyruvate kinase (EC 2.7.1.40).

(Received 20 February 2003, revised 12 May 2003, accepted 4 June 2003)

metal-binding site [11], although other explanations for enzyme inhibition at high metal concentrations have been proposed [12]. Although each of the two active sites appears to be completely independent, attempts to dissociate the enolase have produced inactive monomers, because the subunit interactions are necessary for maintaining the structure of the active site [13].

The enolase reaction is the first step in gluconeogenesis, which is also part of the glycolytic pathway. Many organisms (all vertebrates, *S. cerevisiae*) have different enolase isoenzymes. In vertebrates, the expression of the isoenzymes is regulated both developmentally and tissue specifically, but the kinetic properties of all isoenzymes are very similar [14,15]. In yeast, the levels of the two isoenzymes are under metabolic and developmental control, and the kinetics are specific for an involvement in either the glycolytic or the gluconeogenic pathway [16–18]. All of these differences in tissue distribution, developmental control and activity regulation form important mechanisms to prevent futile cycling.

In this article we report the results of an analysis of *Trypanosoma brucei* enolase. This protozoan organism, living in the bloodstream of humans, is responsible for sleeping sickness, a serious, often fatal, disease of humans in sub-Saharan African countries and for which no adequate drug treatment is available [19,20]. Glycolysis is the sole ATP-yielding metabolic pathway in bloodstream-form trypanosomes, and is therefore perceived as a valid and promising target for the design of new trypanocidal drugs [21]. In this parasite, the first seven enzymes of the glycolytic pathway, involved in the conversion of glucose into 3-phosphoglycerate, are enclosed in peroxisome-like organelles, the glycosomes. The activity of the last three enzymes of the pathway, including enolase, is found predominantly in the cytosol [22,23].

The gene coding for enolase in *T. brucei* has been cloned [24] and its sequence used for a phylogenetic analysis [24,25]. We report here the high-level expression of this *T. brucei* enzyme in *Escherichia coli* and its purification. The kinetic properties of the bacterially expressed enzyme were compared with those of the rabbit muscle and *S. cerevisiae* enolase and with the natural enzyme in a cytosolic fraction of *T. brucei*. Structure modelling, using available three-dimensional enolase structures, showed that some atypical residues close to the active site are potentially interesting for drug design. This prompted us to undertake the structure determination. Crystallization and preliminary crystallographic analysis of the bacterially expressed enzyme are reported.

Materials and methods

Organisms and cell fractionation

Bloodstream forms of *T. brucei* 427 were grown in rats and harvested as described previously [26]. Procyclic trypomastigotes (insect stage cells) were grown in SDM-79 medium at 27 °C [27]. Cell lysates for enzyme assays were prepared by addition of Triton X-100 (0.1%). Cell fractionations, by differential centrifugation and isopycnic sucrose-gradient centrifugation, were carried out essentially as described previously [28].

Construction of a bacterial expression system for *T. brucei* enolase

The complete *T. brucei* enolase gene, without any flanking sequence, was amplified by PCR with two custom-synthesized oligonucleotides: 5′-AGTCTCTACATATGACGAT CCAGA-3′, containing an *Nde*I site (underlined) adjacent to a sequence corresponding to the 5′ end of the enolase gene; and 5′-CGCGGATCCATATCCGTTACGACCA CCGGG-3′, complementary to the 3′-terminal coding region of the gene, followed by a *Bam*HI restriction site (underlined). The amplification mixture (50 μL total volume) contained 1 μg of genomic DNA from *T. brucei* stock 427, 100 pmol of each primer, 250 μM of each of the four deoxynucleotides, and 5 U of r*Taq* DNA polymerase with the corresponding 1 × PCR buffer (TaKaRa, Japan). PCR was performed as follows: an initial incubation at 95 °C for 5 min; 30 cycles of denaturation at 95 °C for 30 s, annealing at 50 °C for 1 min, and extension at 72 °C for 1 min; and a final incubation at 72 °C for 10 min.

The amplified fragment was purified and ligated into pCR2.1-TOPO (Invitrogen). Automated sequencing was then used to check the amplified enolase gene. The gene was subsequently liberated from the recombinant plasmid by digestion with *Nde*I and *Bam*HI and ligated into the expression vector, pET28a (Novagen, USA), which had been predigested with the same enzymes. The new recombinant plasmid directs, under the control of the T7 promoter, the production of a fusion protein bearing an N-terminal extension of 20 residues including a $(His)_6$-tag and a thrombin cleavage site, leaving three amino acids (Gly-Ser-His) in front of the initiator methionine. The *E. coli* BL21(DE3)pLysS strain, which has the T7 RNA polymerase gene under the control of the lacUV5 promoter, was then transformed with the recombinant plasmid.

Protein production and purification

Two purification protocols were developed, the second being used exclusively for protein destined for crystallization.

In the first protocol, the cells harbouring the recombinant plasmid were grown at 37 °C in 50 mL of Luria–Bertani (LB) medium supplemented with 1 M sorbitol, 30 $\mu g \cdot mL^{-1}$ kanamycin and 25 $\mu g \cdot mL^{-1}$ chloramphenicol. Isopropyl thio-β-D-galactoside (IPTG) was added to a final concentration of 1 mM, when the culture reached an absorbance (A) at 600 nm of ≈ 0.5, to induce expression of the protein, and growth was continued overnight at 30 °C. Cells were collected by centrifugation and resuspended in 15 mL of cell lysis buffer [0.05 M triethanolamine/HCl buffer, pH 8, 200 mM KCl, 1 mM KH_2PO_4, 5 mM $MgCl_2$, 0.1% Triton X-100, 1 μM leupeptin, 1 μM pepstatin and 1 μM 4-[(2*S*,3*S*)-3-carboxyoxiran-2-ylcarbonyl-L-leucylamido]butylguanidine (E-64)]. Cells were lysed by two passages through an SLM-Aminco French pressure cell (SLM Instruments Inc.) at 90 MPa. The nucleic acids were removed by incubation with, first, 50 U of benzonase (30 min at 37 °C; Merck) and then protamine sulphate (0.5 $mg \cdot mL^{-1}$; 15 min at room temperature) followed by centrifugation for 10 min at 10 000 ***g***. One millilitre of

washed Metal Affinity Resin (Talon resin; Clontech) was added to the sample and the suspension was mixed on a rotator for 20 min. The resin with bound protein was washed three times (by centrifugation at 700 ***g*** for 5 min) with 10 mL of lysis buffer supplemented with 10 mM imidazole, transferred to a gravity column and washed twice with 3 mL of the same buffer. Finally, the protein was eluted with 5 mL of lysis buffer supplemented with 100 mM imidazole. Purified $(His)_6$-enolase was used for raising polyclonal antiserum in rabbits.

In the second protocol, an identical procedure to the first was adopted up to the point of cell lysis, which was performed in the absence of E-64. Thereafter, the cells were subjected to lysozyme treatment for 30 min on ice prior to freeze-thawing five times and then centrifugation at 10 000 ***g*** for 20 min. The supernatant was applied directly to a Ni-nitrilotriacetic acid affinity resin (Qiagen) pre-equilibrated in the same buffer. After exhaustively washing the column, the bound protein was eluted with a 0–500 mM imidazole gradient.

Thrombin cleavage of the recombinant protein product

The cloning vector used offered the opportunity to cleave the His-tag from the purified protein, dialysed against 0.15 M phosphate-buffered saline ($NaCl/P_i$), pH 7.4, before further use. For this, 1 μL of thrombin solution (1 $U{\cdot}mL^{-1}$) was added for each 20 μg of enolase obtained from the second protocol described above. The cleavage was carried out during a 6 h incubation at 22 °C and stopped by addition of 1 mM phenylmethylsulphonylfluoride. Coomassie-stained SDS/PAGE gels were used to evaluate the success of the His-tag removal.

Protein measurements, SDS/PAGE and Western blotting

Protein concentrations were determined using the Bio-Rad protein assay, based on Coomassie Brilliant Blue [29], with BSA as standard. PAGE in the presence of 0.1% SDS (SDS/PAGE) was performed according to Laemmli [30]. After electrophoresis, the gels were either stained with Coomassie Brilliant Blue, or used for immunoblotting according to the method of Towbin [31]. The membranes were blocked by incubation in $NaCl/P_i$ containing 0.1% Tween-20 and 5% (w/v) low-fat milk powder. For detection of the protein, the primary antibody was diluted (1 : 20 000) in blocking solution. The secondary antibody, anti-rabbit horseradish peroxidase-conjugated Ig (Rockland), was diluted 1 : 40 000 and visualized using the ECL Western Blotting System, a luminol-based system (Amersham Biosciences).

Enzymes and substrates

Rabbit muscle pyruvate kinase (PYK), beef heart lactate dehydrogenase (LDH), rabbit muscle phosphoglycerate mutase (PGAM), yeast 3-phosphoglycerate kinase (PGK), rabbit muscle glyceraldehyde-3-phosphate dehydrogenase (GAPDH), NADH and ADP were purchased from Roche Molecular Biochemicals; PGA, 2,3-bisphosphoglycerate and enolase from bakers yeast and from rabbit muscle were from Sigma; PEP was purchased from Acros Organics (Belgium). The kinetic experiments on *T. brucei* enolase were performed with a cytosolic fraction (post-small-granular fraction [28]) from a cell extract containing the natural enzyme and with the purified His-tagged bacterially expressed protein.

The concentration of PGA was determined enzymatically with rabbit muscle enolase, PYK and LDH. PEP concentrations were determined enzymatically using rabbit muscle enolase, PGAM, PGK and GAPDH.

Enzyme assay and kinetic studies

For routine measurements, the enolase activity was measured by coupling its reaction to PYK and LDH and by following the decrease of NADH absorbance at 340 nm using a Beckman DU7 spectrophotometer. This standard assay was performed at 25 °C in a 1.0 mL reaction mixture containing 0.1 M triethanolamine/HCl, pH 7.6, 1 mM PGA, 1.1 mM ADP, 0.42 mM NADH, 2 mM $MgSO_4$ and 17 mM KCl. The auxiliary enzymes – PYK and LDH – were used at final activities of 2 and 1.2 $U{\cdot}mL^{-1}$, respectively. One activity unit is defined as the conversion of 1 μmol $substrate{\cdot}min^{-1}$ under these standard conditions.

The Michaelis constant (K_m) of enolase for PGA was determined using the above-mentioned reaction conditions, by varying the concentration of PGA between 3 μM and 3 mM. To determine the K_m for its substrate in the reverse reaction, the assays were performed in a reaction mixture containing 0.1 M triethanolamine/HCl, pH 7.6, 1 mM ATP, 0.42 mM NADH, 0.1 mM 2,3-*bis*phosphoglycerate, 2 mM $MgSO_4$ and 1 mM dithiothreitol and, as auxiliary enzymes, PGAM, PGK and GAPDH, at final concentrations of 2 $U{\cdot}mL^{-1}$, 25 $\mu g{\cdot}mL^{-1}$ and 8 $U{\cdot}mL^{-1}$, respectively. The K_m for PEP was determined by varying its concentration between 8 μM and 4 mM. Kinetic parameters were calculated from Michaelis–Menten plots by curve-fitting of experimentally determined data, using the SIGMAPLOT program.

To study the effect of pH, the triethanolamine buffer in the standard assay was replaced with 50 mM Mes, Hepes, 2-(*N*-cyclohexylamino)ethanesulfonic acid or Caps buffers; the pH was adjusted with KOH, and KCl was added to give a final ionic strength of 0.1 M, as described previously [32].

For studies of activation and inhibition by monovalent and divalent ions, the reaction mixture was the same as in the standard assay, but Mg^{2+} was omitted. Different salts at varying concentration were added, as follows: $MgSO_4$ (0–160 mM); KCl, NaCl and LiCl (0–0.5 M); $CoCl_2$, $MnCl_2$ and $CuCl_2$ (0–200 μM). From the experimental data thus obtained, K_a and K_i^{app} for Mg^{2+} were determined by a best fit to the following equation for substrate inhibition [33]:

$$v = [V_{max} \times [S]/(K_a + [S] + ([S] \times [S]/K_i)],$$

where $S = Mg^{2+}$ and V_{max} = maximal rate.

Control experiments for each set of assays showed that the auxilliary enzymes were not a limiting factor and that the rate of the reaction was a function of the concentration of enolase.

Alignment of sequences and structure modelling of *T. brucei* enolase

A sequence alignment of *T. brucei* enolase with other validated bacterial and eukaryotic enolases from the ENZYME database [34] was made with CLUSTAL W [35]. Within the resulting alignment of 52 enolases, positions were sought at which the *T. brucei* sequence possessed an unusual amino acid, unique within the sequence set or shared by only a few other sequences.

Structures of enolases from three different species – *Homarus vulgaris* (lobster [6]), *S. cerevisiae* [8] and *E. coli* [36] – were available as potential templates for model construction. *T. brucei* enolase shares 58, 59 and 51% sequence identity, respectively, with these three enolases. *S. cerevisiae* enolase structures were therefore chosen as templates although the strong structural similarity shared by all known enolase structures [36] ensured that the choice of template would not have a large impact on the probable accuracy of the *T. brucei* enolase models. Insertions and deletions in the *T. brucei* sequence, relative to that of *S. cerevisiae*, were positioned between secondary structural elements and models constructed with MODELLER [37]. Separate models were constructed for substrate-bound *T. brucei* enolase conformations with one or two Mg^{2+} atoms based, respectively, on the structures with PDB codes 7enl [7] and 1ebg [38]. STRIDE [39] was used for the definition of secondary structure in the models and DSSP [40] for solvent-accessibility measurements.

Dynamic light scattering

The hydrodynamic radius of the purified protein (both before and after His-tag removal) was estimated by Dynamic Light Scattering measurements using a DynaPro MS800 instrument (Protein Solutions, Lakewood, NJ, USA). All solutions were centrifuged at 10 000 ***g*** for 20 min prior to data collection. Data were acquired by accumulation of 50 scans of ≈ 2.0 s with the laser intensity set to 50–60% maximum, and the particle size distribution was calculated using the software package DYNAMICS supplied with the instrument.

Crystallization and preliminary crystallographic analysis of *T. brucei* enolase

After thrombin treatment for removal of the His-tag, the protein was concentrated using centriprep and/or centricon 10 000 (Amicon) concentrators to a maximum final concentration of 6 $mg{\cdot}mL^{-1}$. Sparse matrix crystallization trials were carried out using the Crystal Screen kits – Crystal Screen I and II – from Hampton Research (Laguna Hills, CA, USA). The hanging drop method was used, with drops comprising 3 μL of protein mixed with 3 μL of trial solution suspended over 500 μL of trial solution. The crystallization plates were mounted and incubated at 18 °C.

Diffraction patterns for the crystals were obtained using a RIGAKU UltraX 18 generator (RIGAKU Corporation, Tokyo, Japan) coupled to a MAR345 image plate detector (X-ray Research GmbH, Norderstedt, Germany). Data were processed using the Automar program (X-ray Research GmbH).

Results and discussion

Enolase activity in *T. brucei* and subcellular distribution

Bloodstream-form *T. brucei* is entirely dependent on glycolysis for its ATP supply. The glycolytic flux in these cells occurs at a relatively high rate, whereas procyclic insect-stage trypanosomes, as a result of an active mitochondrial metabolism, have a much lower capacity to consume glucose [reviewed in refs 41,42]. Previously, it has been shown that some glycolytic enzymes (e.g. triosephosphate isomerase and aldolase) have a similar level of specific activity in both life cycle stage forms, whereas for others (e.g. hexokinase and pyruvate kinase) the levels differ considerably [43]. Such information is, to date, not available for enolase. Therefore, we measured the activity of this enzyme in both cell types. The specific activity was 4.5-fold higher in a total homogenate of bloodstream-form trypanosomes (768 $mU{\cdot}mg\ protein^{-1}$) than in a cultured procyclic trypomastigote homogenate (169 $mU{\cdot}mg\ protein^{-1}$). An approximate fivefold difference was also detected by Western blots (Fig. 1), indicating that the specific activity difference should be attributed to developmentally regulated expression of the enzyme during the life cycle.

Previous work has located most enolase activity in bloodstream-form *T. brucei* in the cytosol [22,23]. We decided to reanalyze, in a more detailed manner, the subcellular localization of enolase. Therefore, different subcellular fractions of *T. brucei* procyclic and bloodstream forms were prepared by differential centrifugation. These fractions were then subjected to SDS/PAGE, blotted and probed with a polyclonal antiserum raised against the purified, bacterially expressed enolase. As shown in Fig. 1, enolase was found only in the soluble fraction of both bloodstream-form and procyclic trypanosomes. This analysis was then refined, through further fractionation of the post large-granular fraction, by isopycnic centrifugation in a sucrose gradient. Figure 2 shows the distribution profiles of several enzymes of a *T. brucei* bloodstream-form homogenate. This analysis confirms the predominant localization of the enolase in the cytosol as this enzyme fractionated together with the cytosolic enzyme, PGAM [44], at the top

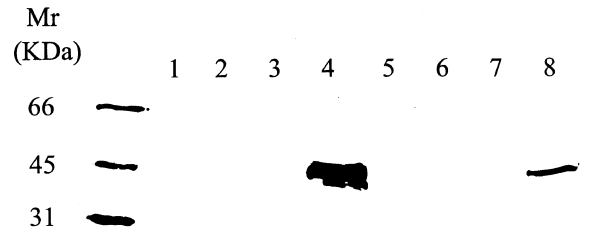

Fig. 1. Subcellular localization of enolase. A *T. brucei* bloodstream form (lanes 1–4) and procyclic trypomastigote (lanes 5–8) homogenates were separated by differential centrifugation into large granular (LG) (lanes 1 and 5), small granular (SG) (lanes 2 and 6), microsomal (M) (lanes 3 and 7) and cytosolic (C) (lanes 4 and 8) fractions. Twenty micrograms of protein was loaded per well. The fractions were analysed by SDS/PAGE and Western blotting, using polyclonal anti-enolase serum.

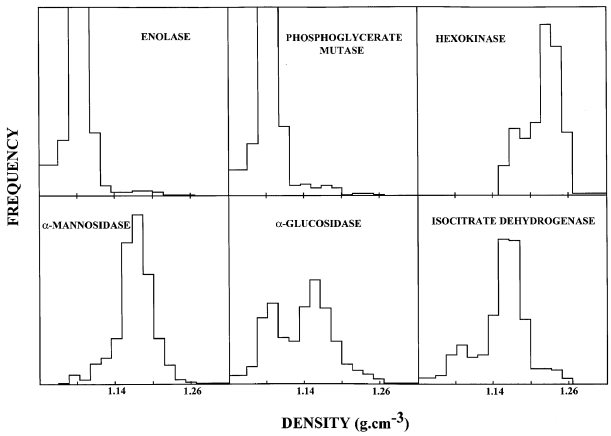

Fig. 2. Distribution profiles of the post large-granular fraction of a homogenate of bloodstream-form *T. brucei* after isopycnic centrifugation on a linear sucrose gradient. The fractions were assayed for enolase and the following marker enzyme activities: phosphoglycerate mutase (PGAM) (cytosol), hexokinase (glycosomes), α-mannosidase (lysosomes), α-glucosidase (plasma membrane) and isocitrate dehydrogenase (mitochondrion). The presentation of the distribution profiles is as described by Beaufay & Amar-Costesec [50].

of the gradient, whereas no activity at all cosedimented with the glycosomal hexokinase at a density of 1.23 g·cm^{-3}.

Expression of *T. brucei* enolase in *E. coli*, purification of the enzyme and kinetic analysis

The *T. brucei* enolase expressed in *E. coli* could be purified 48.5-fold to homogeneity, as assessed by SDS/PAGE, having a specific activity of 85.4 U·mg^{-1}, with a yield of 1.9 mg from a 50 mL culture of recombinant bacteria.

Kinetic parameters were determined by systematic variation of each of the substrates. The results are listed in Table 1. Under the conditions described above, the following K_m values were measured for the bacterially expressed *T. brucei* enolase: for the forward reaction, $K_m = 54$ μM for the substrate PGA; for the reverse reaction, $K_m = 244$ μM for PEP. These affinities are within the same range as measured for the natural *T. brucei*, yeast and rabbit muscle enolases.

The effect of pH on the reaction with PGA was studied for the bacterially expressed trypanosomal enolase and compared with that of its homologues from rabbit muscle and yeast. Various buffers were used at different pH values, while maintaining a constant ionic strength of 0.1 M. A bell-shaped relationship between pH and activity was found, with maximal activity at pH 7.7 for the *T. brucei* enolase and at pH 7.0 and 7.5 for the mammalian and the yeast enzymes, respectively. Outside the pH range 7.3–8.0, the activity of the *T. brucei* enolase decreased steadily, with 60% activity remaining at pH 7.0 and 50% at pH 8.4. The lower pH optimum observed for the rabbit muscle enolase might probably explained by a difference in metal ion affinity, as an increased inhibition by Mg^{2+} above pH 7.1 was reported for this enzyme [45].

Mg^{2+} is essential for enolase activity, but at high concentrations inhibits the enzyme. Comparable K_a values have been obtained for all enolases studied and K_i^{app} values are similar between the *T. brucei* and yeast enzymes (Table 1). Rabbit muscle enolase is more susceptible to inhibition by an excess of Mg^{2+} than the two other enzymes, at least at the pH (7.6) used in this study, in accordance with the observation that metal ion binding by this enzyme is strongly influenced by pH [45]. Moreover, two processes seem to contribute to inhibition: the first, with an apparent K_i^{app} of 7.5 mM, leading to a reduced activity of about 40%, is followed by a second with a K_i^{app} of > 100 mM. This observation was not made for the *T. brucei* and yeast enzymes. Co^{2+}, Mn^{2+} and Cu^{2+} inhibit all enolases studied. Monovalent cations also affect the activity of the enzymes. Li^+ and Na^+ inhibit them all; rabbit enolase is activated by K^+, but *T. brucei* and yeast enolase are not.

Comparable kinetic properties and Mg^{2+} dependence between the two *T. brucei* enolase preparations strongly indicate that the expression system used, in addition to providing a simple method for obtaining large amounts of purified protein, also produces the enzyme in the fully active form, with no apparent differences from the natural *T. brucei* enolase.

Comparison of the *T. brucei* enolase sequence with the sequences of the corresponding protein in other organisms

The cloning and characterization of the *T. brucei* enolase gene has been described previously [24]. It encodes a polypeptide of 428 amino acids (excluding the initiator methionine) with a relative molecular mass of 46 461. The trypanosomal sequence shows 58–63% identity with other (nontrypanosomatid) eukaryotic sequences and 46–52% identity with all prokaryotic sequences, including enolase of spirochaetes (*Treponema palladium*, 51% identity) that appeared phylogenetically most related to the *T. brucei* sequence [24]. In addition, an identity of 78% was found with the sequence of the related trypanosomatid *Leishmania major*. The identity of *T. brucei* enolase with the

Table 1. Kinetic properties of enolase from different sources. The experimental errors were within 10%. SA, specific activity.

Source of enzyme	SA PGA (U·mg^{-1})	K_m PGA (μM)	SA PEP (U·mg^{-1})	K_m PEP (μM)	K_a Mg^{2+} (mM)	K_i^{app} Mg^{2+} (mM)
T. brucei (from *E. coli*)	63	53.8	6.3	244	0.45	50
T. brucei (natural)		49.1		289	0.36	67
Rabbit muscle	31	16.2	6.4	238	0.26	7.5/100
Yeast	65	57.0	7.8	264	0.43	43

three isoenzymes of the parasite's human host is 59–62%. These overall identity values are higher than observed for any other trypanosomatid glycolytic enzyme [21]. The comparison revealed that the residues essential for the catalytic activity, as well as those constituting the binding sites of substrates and two Mg^{2+} ions, are invariably present in all sequences (Fig. 3). The *T. brucei* sequence has a unique amino acid at 29 positions. In a further 22 positions, the trypanosomal residue is shared by just one other sequence. These positions were visualized through molecular modelling.

Determinations of various metal and substrate complexes of *S. cerevisiae* enolase have enabled the formulation of a detailed proposed catalytic mechanism [7,46]. There are three loops that differ significantly in position between apoenzyme and holoenzyme structures: two within the large domain; the third contributed by the smaller domain. The structures have shown that little change in loop conformations, relative to the apoenzyme structure (Protein Data Bank code 3enl [4]), accompanies occupation of the first, high-affinity divalent cation-binding site (1ebh [38]). These are termed the open-loop structures. A very large change accompanies binding of substrate (7enl [7]); and a further change occurs on binding to the second divalent cation-binding site of the catalytic site [47]. These are the closed-loop structures.

Modelling of *T. brucei* enolase, in both open- and closed-loop forms, showed that the atypical residues of the trypanosome enzyme are predominantly found at the protein surface. At least one-third seem to be clustered on one particular face, largely composed of α-helices, distant from the catalytic sites and dimer interface. The particular function, if any, of this region is unknown.

With the benefit of the model, steric and chemical differences between trypanosomal and mammalian enolases near the catalytic site, which might facilitate the design of species-specific inhibitors, were sought. The nearest atypical residue to the catalytic site is Lys155, which replaces a serine in most enzymes, including the human enolase. As shown in Fig. 4(A), this lysine, in a favourable extended conformation, is suitably placed to interact with the substrate in the enzyme structure bound to a single divalent cation. In contrast, after binding of the catalytically essential second divalent cation, with concomitant repositioning of neighbouring His156 to interact with the phospho group, the models show that this lysine may no longer interact with the ligand (Fig. 4B). The prediction that Lys155 (present only in trypanosomatids *T. brucei* and *L. major*, *Euglena gracilis* and *Treponema pallidum* sequences) could interact with catalytic site-bound ligand, albeit not in the catalytically competent enzyme conformation, is important as its side-chain primary amine group could be irreversibly covalently

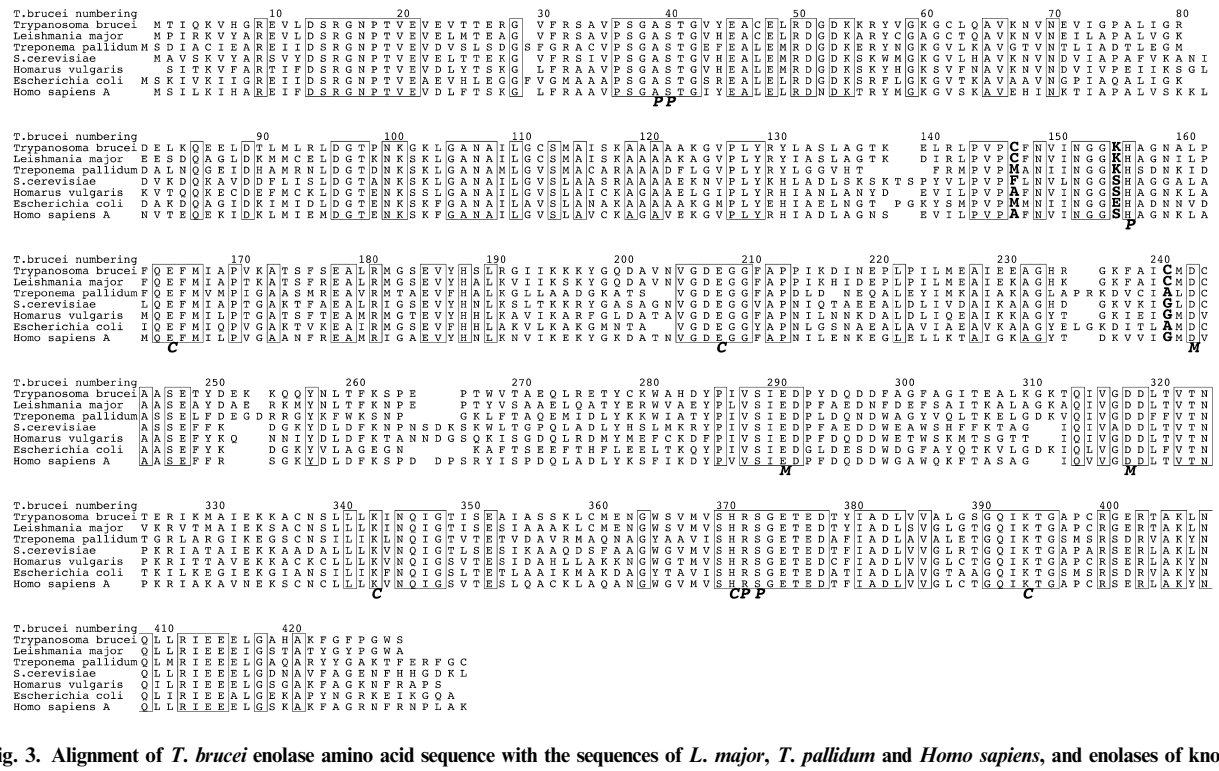

Fig. 3. Alignment of *T. brucei* enolase amino acid sequence with the sequences of *L. major*, *T. pallidum* and *Homo sapiens*, and enolases of known three-dimensional structure. Genepept accession numbers for the sequences of the alignment are as follows: *T. brucei* (8132069), *L. major* (8388689), *T. pallidium* (4033380), *Saccharomyces cerevisiae* (119336), *Homarus vulgaris* (3023703), *E. coli* (1706655) and *H. sapiens* (119339). Boxes mark identities and large bold type is used for the three residues, discussed in detail in the text, whose modification may offer a route to irreversible inhibition of *T. brucei* enolase. The letters below the alignment mark residues involved in binding to the phospho or carboxyl groups of substrate phospho*enol*pyruvate (PEP) (P and C, respectively) or to the first metal site, common to both open- and closed-loop structures (M). The figure was produced using ALSCRIPT [51].

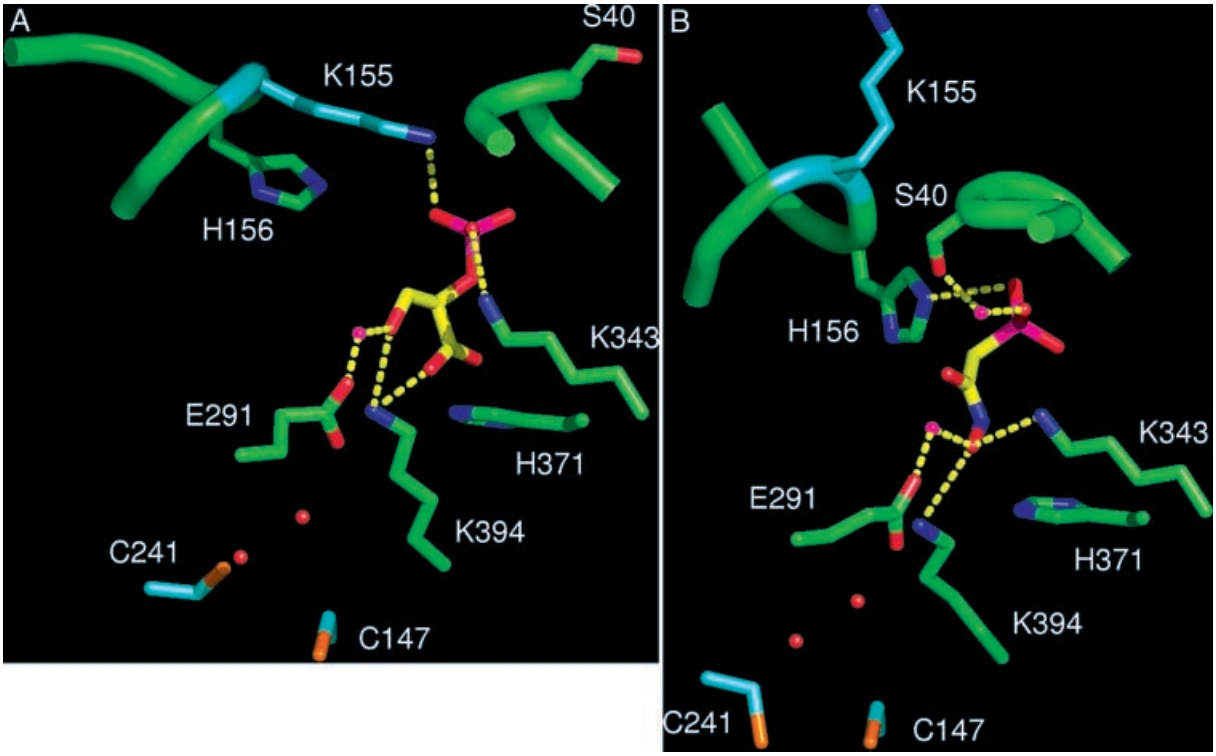

Fig. 4. Active site models of *T. brucei* enolase. PYMOL [52] figures of the *T. brucei* enolase models were prepared based on (A) the substrate, single Mg^{2+} complex of *Saccharomyces cerevisiae* enolase (PDB code 7enl [7]); and (B) the inhibitor phosphonoacetohydroxamate, double Mg^{2+} complex (PDB code 1ebg [38]). Carbon atoms of putative targets for irreversible inhibition are shown in cyan and discussed in detail in the text. Carbon atoms of the ligand are shown in yellow, water atoms (see text) are drawn as isolated red spheres, and magnesium ions as isolated magenta spheres. Electrostatic interactions are indicated with dotted yellow lines. Backbone traces are shown for regions that adopt significantly different conformations in the two models. The different side-chain conformations of Cys241 reflect genuine uncertainty as this residue replaces a glycine in the templates. For clarity, not all ligand interactions are shown.

bound to a suitable inhibitor, permanently disabling the trypanosomal enolase. It is important to note that kinetic evidence suggests that binding of the second divalent cation is dependent on the presence of substrate so that the enzyme must necessarily pass through the substrate-single M^{2+} state during the catalytic cycle [12]. It is therefore a valid conformational state for drug targeting. The possible interaction of Lys155 with substrate during the catalytic cycle is currently the subject of crystallographic studies.

The next nearest atypical residue to the catalytic site is at position 241 where all the other enzymes have an alanine or a glycine, but *T. brucei* and *L. major* have a cysteine. This amino acid is near position 147, where alanine, methionine and phenylalanine are frequently present but where *T. brucei* also has a cysteine, in common only with *L. major*, *Entamoeba histolytica* and *Plasmodium falciparum*. Although predicted to lie close to one another, the cytosolic location of enolase, with its low redox potential, ensures that the formation of a disulphide bridge between them is extremely unlikely. These cysteines may also offer interesting possibilities for the design of selective inhibitors, although their presence in the second shell of the catalytic site, rather than in the first (Fig. 4) raises doubts as to their accessibility to potentially reactive ligands. However, two factors offer support for their being at least partially accessible. First, Cys147, completely buried from solvent in the *T. brucei* enolase models, gains solvent accessibility if side-chain mobility of Lys394 is simulated by its replacement with alanine. Second, in the region below Lys394 in the *S. cerevisiae* enolase crystal structures, two water molecules are present (Fig. 4). Modelling suggests that this cavity is also predicted to exist in the *T. brucei* enolase. Although buried, nonexchanging solvent molecules are known to exist in protein structures, relatively modest movement of Lys394 and Glu291 side-chains would allow these water molecules to exchange with bulk solvent. The same motions would be expected to allow access to suitably sized irreversible *T. brucei* enolase inhibitors.

Crystallization and preliminary crystallographic analysis of *T. brucei* enolase

With the clear potential for species-specific inhibitors of *T. brucei* enolase established, we initiated attempts to determine its three-dimensional structure by X-ray crystallography.

In order to determine whether the original His-tagged protein or the thrombin-cleaved version offered the better chance of crystallization, we used the dynamic light-scattering technique [49]. The ability of dynamic light scattering to detect aggregates in a protein solution, whose

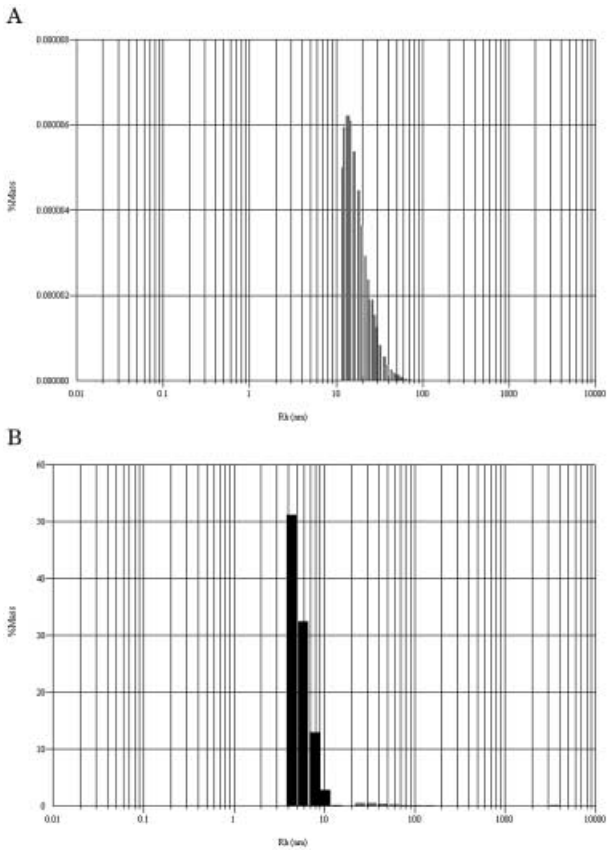

Fig. 5. The presence of a His-tag augments the inclination of *T. brucei* enolase to form aggregates. Light scattering data show the formation of aggregates upon concentration of the His-tagged enolase (A) but a near-monodisperse solution (containing only around 2% aggregates) for the concentrated cleaved enzyme (B).

presence impedes crystallization, has led to its increasing adoption as a screen for conditions in which a given protein is ideally monodisperse. In the case of *T. brucei* enolase, the original His-tagged protein showed a marked inclination to aggregate upon concentration of 4 $mg{\cdot}mL^{-1}$ (Fig. 5A), in contrast to the thrombin-cleaved protein, for which only $\approx 2\%$ of protein was present in aggregated forms (Fig. 5B). Crystallization trials were therefore carried out with the thrombin-cleaved enolase preparation, as reported above. After ≈ 10 days, hexagonal crystals were obtained in condition 27 of Crystal Screen II containing the following: 0.01 M zinc sulphate, 0.1 M Mes, pH 6.5, and 25% (v/v) poly(ethylene glycol) monomethylether 550. Diffraction data obtained to 2.3 Å revealed a space group of $C222_1$ (a = 74.02 Å, b = 110.54 Å and c = 109.10 Å), and structure solution by molecular replacement is underway.

Conclusion

We have shown that, in *T. brucei*, enolase is present only in the cytosol. Its expression is developmentally regulated; the specific cellular activity is 4.5-fold higher in bloodstream-form parasites than in cultured procyclic cells. The *T. brucei* enzyme has been expressed in *E. coli* and subjected to a kinetic analysis. The parasite enzyme has kinetic properties similar to those of yeast and the natural *T. brucei* enolases. A different pH optimum and inhibition by an excess of Mg^{2+} have been observed for the rabbit-muscle enzyme. The overall amino acid identity of the trypanosome enolase with its counterpart in other organisms is relatively high compared with that of other glycolytic enzymes. Nevertheless, inspection of its amino acid sequence and modelling of its three-dimensional structure revealed three atypical residues – one Lys and two Cys – close to the active site. These residues are shared with another pathogenic trypanosomatid, *L. major*. The presence of these unique residues offers interesting opportunities for the design of inhibitors selective for the enzyme of these related parasites. The availability of *T. brucei* enolase crystals diffracting at high resolution will permit us to pursue the structure resolution.

Acknowledgements

The authors would like to acknowledge Anne Diederich (ICP, Brussels) and Luciane Vieira de Mello (Cenargen/Embrapa, Brasília) for their contributions to the work reported in this article. This study was financially supported by the European Commission through its INCO-DEV programme (contract ICA4-CT-2001-10075) and by the Université Catholique de Louvain through an 'Action de recherche concerté'.

References

1. Wold, F. (1971) Enolase. In *The Enzymes*, Vol. 5 (Boyer, P.D., ed.), pp. 499–538. Academic Press, New York, USA.
2. Schurig, H., Rutkat, K., Rachel, R. & Jaenicke, R. (1995) Octameric enolase from the hyperthermophilic bacterium *Thermotoga maritima*: purification, characterization, and image processing. *Protein Sci.* **4**, 228–236.
3. Brown, C.K., Kuhlman, P.L., Mattingly, S., Slates, K., Calie, P.J. & Farrar, W.W. (1998) A model of the quaternary structure of enolases, based on stuctural and evolutionary analysis of the octameric enolase from *Bacillus subtilis*. *Protein Chem.* **17**, 855–866.
4. Stec, B. & Lebioda, L. (1990) Refined structure of yeast apoenolase at 2. 25-Å resolution. *J. Mol. Biol.* **211**, 235–248.
5. Lebioda, L. & Stec, B. (1991) Mechanism of enolase: the crystal structure of enolase-Mg^{2+}-2-phosphoglycerate/phosphoenolpyruvate complex at 2.2-Å resolution. *Biochemistry* **30**, 2817–2822.
6. Duquerroy, S., Camus, C. & Janin, J. (1995) X-ray structure and catalytic mechanism of lobster enolase. *Biochemistry* **34**, 12513–12523.
7. Zhang, E., Brewer, J.M., Minor, W., Carreira, L.A. & Lebioda, L. (1997) Mechanism of enolase: the crystal structure of asymmetric dimer enolase-2-phospho-D-glycerate/enolase phosphoenolpyruvate at 2.0 Å resolution. *Biochemistry* **36**, 12526–12534.
8. Lebioda, L., Stec, B. & Brewer, J.M. (1989) The structure of yeast enolase at 2.25-Å resolution. An 8-fold $\beta + \alpha$-barrel with a novel $\beta\beta\alpha\alpha$ $(\beta\alpha)_6$ topology. *J. Biol. Chem.* **264**, 3685–3693.
9. Elliott, J.I. & Brewer, J.M. (1980) Binding of inhibitory metals to yeast enolase. *J. Inorg. Biochem.* **12**, 323–334.
10. Lee, B.H. & Nowak, T. (1992) Influence of pH on the Mn^{2+} activation of and binding to yeast enolase: a functional study. *Biochemistry* **31**, 2165–2171.
11. Faller, L.D., Baroudy, B.M., Johnson, A.M. & Ewall, R.X. (1977) Magnesium ion requirements for yeast enolase activity. *Biochemistry* **16**, 3864–3869.
12. Poyner, R.R., Cleland, W.W. & Reed, G.H. (2001) Role of metal ions in catalysis by enolase: an ordered kinetic mechanism for a single substrate enzyme. *Biochemistry* **40**, 8009–8017.

13. Kornblatt, M.J., Lange, R. & Balny, C. (1998) Can monomers of yeast enolase have enzymatic activity? *Eur. J. Biochem.* **251**, 775–780.
14. Tanaka, M., Sugisaki, K. & Nakashima, K. (1985) Switching in levels of translatable mRNAs for enolase isozymes during development of chicken skeletal muscle. *Biochem. Biophys. Res. Commun.* **133**, 868–872.
15. Segil, N., Shrutkowski, A., Dworkin, M.B. & Dworkin-Rastl, E. (1988) Enolase isoenzymes in adult and developing *Xenopus laevis* and characterization of a cloned enolase sequence. *Biochem. J.* **251**, 31–39.
16. McAlister, L. & Holland, M.J. (1982) Targeted deletion of a yeast enolase structural gene. Identification and isolation of yeast enolase isozymes. *J. Biol. Chem.* **257**, 7181–7188.
17. Etian, K.-D., Fröhlich, K.-U. & Mecke, D. (1984) Regulation of enzymes and isoenzymes of carbohydrate metabolism in the yeast *Saccharomyces cerevisiae*. *Biochim. Biophys. Acta* **799**, 181–186.
18. Etian, K.-D., Meurer, B., Köhler, H., Mann, K.-H. & Mecke, D. (1987) Studies on the regulation of enolases and compartmentation of cytosolic enzymes in *Saccharomyces cerevisiae*. *Biochim. Biophys. Acta* **923**, 214–221.
19. World Health Organization (2001) *WHO Fifteenth Programme Report: UNDP/World Bank/WHO Special Programme for Research and Training in Tropical Diseases (TDR)*. WHO, Geneva, Switzerland.
20. Gelb, M.H. & Hol, W.G.J. (2002) Drugs to combat tropical protozoan parasites. *Science* **297**, 343–344.
21. Verlinde, C.L., Hannaert, V., Blonski, C., Willson, M., Périé, J.J., Fothergill-Gilmore, L.A., Opperdoes, F.R., Gelb, M.H., Hol, W.G.J. & Michels, P.A.M. (2001) Glycolysis as a target for the design of new anti-trypanosome drugs. *Drug Resist. Updat.* **4**, 50–65.
22. Opperdoes, F.R. & Borst, P. (1977) Localization of nine glycolytic enzymes in a microbody-like organelle in *Trypanosoma brucei*: the glycosome. *FEBS Lett.* **143**, 360–364.
23. Oduro, K.K., Bowman, I.B.R. & Flynn, I.W. (1980) *Trypanosoma brucei*: preparation and some properties of a multienzyme complex catalysing part of the glycolytic pathway. *Exp. Parasitol.* **50**, 240–250.
24. Hannaert, V., Brinkmann, H., Nowitzki, U., Lee, A.J., Albert, M.-A., Sensen, C.W., Gaasterland, T., Müller, M., Michels, P. & Martin, W. (2000) Enolase from *Trypanosoma brucei*, from the amitochondriate protist *Mastigamoeba balamuthi*, and from the chloroplast and cytosol of *Euglena gracilis*: pieces in the evolutionary puzzle of the eukaryotic glycolytic pathway. *Mol. Biol. Evol.* **17**, 989–1000.
25. Keeling, P.J. & Palmer, J.D. (2000) Parabasalian flagellates are ancient eukaryotes. *Nature* **405**, 635–637.
26. Opperdoes, F.R., Aarsen, P.N., Van der Meer, C. & Borst, P. (1976) *Trypanosoma brucei*: an evaluation of salicylhydroxamic acid as a trypanocidal drug. *Exp. Parasitol.* **40**, 198–206.
27. Brun, R. & Schönenberger, M. (1979) Cultivation and *in vitro* cloning of procyclic forms of *Trypanosoma brucei* in a semi-defined medium. *Acta Trop.* **36**, 289–292.
28. Steiger, R.F., Opperdoes, F.R. & Bontemps, J. (1980) Subcellular fractionation of *Trypanosoma brucei* bloodstream forms with special reference to hydrolases. *Eur. J. Biochem.* **105**, 163–175.
29. Bradford, M.M. (1976) A rapid and sensitive method for the quantitation of microgram quantities of protein utilizing the principle of protein-dye binding. *Anal. Biochem.* **72**, 248–254.
30. Laemmli, U.K. (1970) Cleavage of stuctural proteins during assembly of the head of bacteriophage T4. *Nature* **227**, 680–685.
31. Towbin, H., Staehelin, T. & Gordon, J. (1979) Electrophoretic transfer of proteins from polyacrylamide gels to nitrocellulose sheets: procedure and some applications. *Proc. Natl Acad. Sci. USA* **76**, 4350–4354.
32. Lambeir, A.-M., Loiseau, A.M., Kuntz, D.A., Vellieux, F.M., Michels, P.A.M. & Opperdoes, F.R. (1991) The cytosolic and glycosomal glyceraldehyde-3-phosphate dehydrogenase from *T. brucei*. Kinetic properties and comparison with homologous enzymes. *Eur. J. Biochem.* **198**, 429–435.
33. Cleland, W.W. (1970) Statistical analysis of enzyme kinetic data. *Methods Enzymol.* **63**, 103–138.
34. Bairoch, A. (2000) The ENZYME database in 2000. *Nucleic Acids Res.* **28**, 304–305.
35. Higgins, D., Thompson, J., Gibson, T., Thompson, J.D., Higgins, D.G. & Gibson, T.J. (1994) CLUSTAL W: improving the sensitivity of progressive multiple sequence alignment through sequence weighting, position-specific gap penalties and weight matrix choice. *Nucleic Acids Res.* **22**, 4673–4680.
36. Kuhnel, K. & Luisi, B.F. (2001) Crystal structure of the *Escherichia coli* RNA degradosome component enolase. *J. Mol. Biol.* **313**, 583–592.
37. Sali, A. & Blundell, T.L. (1993) Comparative protein modelling by satisfaction of spatial restraints. *J. Mol. Biol.* **234**, 779–815.
38. Wedekind, J.E., Reed, G.H. & Rayment, I. (1995) Octahedral coordination at the high-affinity metal site in enolase: crystallographic analysis of the MgII–enzyme complex from yeast at 1.9-Å resolution. *Biochemistry* **34**, 4325–4330.
39. Frishman, D. & Argos, P. (1995) Knowledge-based protein secondary structure assignment. *Proteins* **23**, 566–579.
40. Kabsch, W. & Sander, C. (1983) Dictionary of protein secondary structure: pattern recognition of hydrogen-bonded and geometrical features. *Biopolymers* **22**, 2577–2637.
41. Opperdoes, F.R. (1987) Compartmentation of carbohydrate metabolism in trypanosomes. *Annu. Rev. Microbiol.* **41**, 127–151.
42. Michels, P.A.M., Hannaert, V. & Bakker, B.M. (1996) Glycolysis of kinetoplastida. In *Trypanosomiasis and Leishmaniasis: Biology and Control* (Hide, G., Mottram, J.C., Coombs, G.H. & Holmes, P.H., eds), pp. 133–148. CAB International, Wallingford, UK.
43. Hart, D.T., Misset, O., Edwards, S.W. & Opperdoes, F.R. (1984) A comparison of the glycosomes (microbodies) isolated from *Trypanosoma brucei* bloodstream form and cultured procyclic trypomastigotes. *Mol. Biochem. Parasitol.* **12**, 25–35.
44. Chevalier, N., Rigden, D.J., Van Roy, J., Opperdoes, F.R. & Michels, P.A.M. (2000) *Trypanosoma brucei* contains a 2,3-bisphosphoglycerate independent phosphoglycerate mutase. *Eur. J. Biochem.* **267**, 1464–1472.
45. Kornblatt, M.J. & Klugerman, A. (1989) Characterization of the enolase isozymes of rabbit brain: kinetic differences between mammalian and yeast enolases. *Biochem. Cell. Biol.* **67**, 103–107.
46. Reed, G.H., Poyner, R.R., Larsen, T.M., Wedekind, J.E. & Rayment, I. (1996) Structural and mechanistic studies of enolase. *Curr. Opin. Struct. Biol.* **6**, 736–743.
47. Wedekind, J.E., Poyner, R.R., Reed, G.H. & Rayment, I. (1994) Chelation of serine 39 to Mg^{2+} latches a gate at the active site of enolase: structure of the bis(Mg^{2+}) complex of yeast enolase and the intermediate analog phosphonoacetohydroxamate at 2.1-Å resolution. *Biochemistry* **33**, 9333–9342.
48. Lopez, C., Chevalier, N., Hannaert, V., Rigden, D.J., Michels, P.A.M. & Ramirez, J.L. (2002) *Leishmania donovani* phosphofructokinase. Gene characterization, biochemical properties and structure-modelling studies. *Eur. J. Biochem.* **269**, 3978–3989.
49. Ferre-D'Amare, A.R. & Burley, S.K. (1997) Dynamic light scattering in evaluating crystallizability of macromolecules. *Methods Enzymol.* **276**, 157–166.
50. Beaufay, H. & Amar-Costesec, A. (1976) Cell fractionation techniques. In *Methods Mem. Biol.*, Vol. 6 (Korn, E.D., ed.), pp. 1–100. Plenum Press, New York.
51. Barton, G.J. (1993) ALSCRIPT: a tool to format multiple sequence alignments. *Protein Eng.* **6**, 37–40.
52. DeLano, W.L. (2002) The PyMOL Molecular Graphics System on World Wide Web: http://www.pymol.org